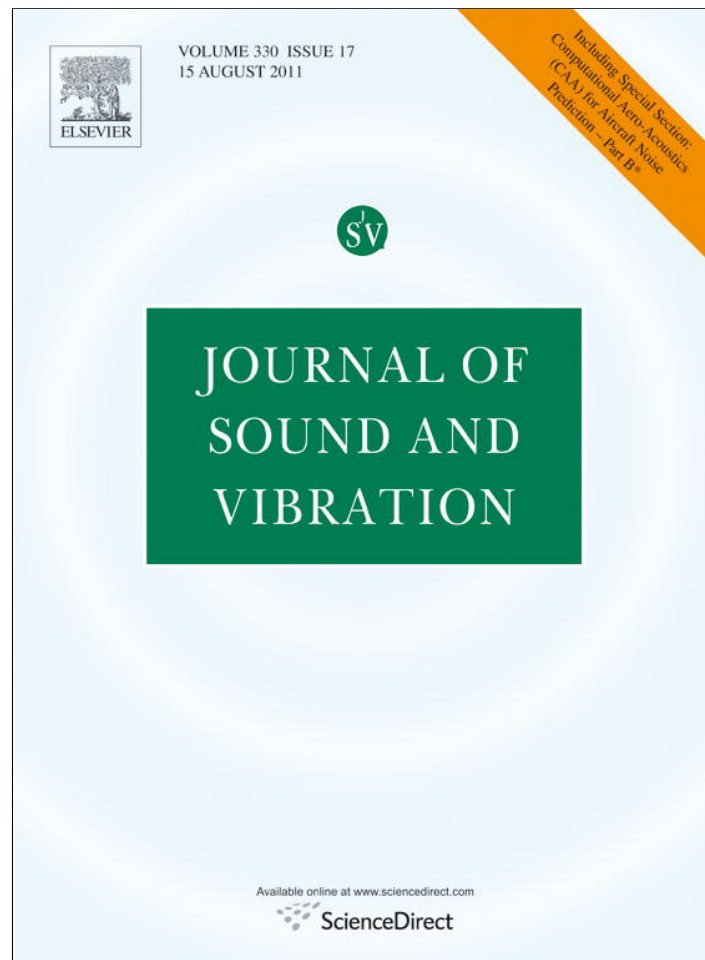


Provided for non-commercial research and education use.
Not for reproduction, distribution or commercial use.



This article appeared in a journal published by Elsevier. The attached copy is furnished to the author for internal non-commercial research and education use, including for instruction at the authors institution and sharing with colleagues.

Other uses, including reproduction and distribution, or selling or licensing copies, or posting to personal, institutional or third party websites are prohibited.

In most cases authors are permitted to post their version of the article (e.g. in Word or Tex form) to their personal website or institutional repository. Authors requiring further information regarding Elsevier's archiving and manuscript policies are encouraged to visit:

<http://www.elsevier.com/copyright>



Contents lists available at ScienceDirect

Journal of Sound and Vibration

journal homepage: www.elsevier.com/locate/jsvi

LES-based evaluation of a microjet noise reduction concept in static and flight conditions[☆]

Mikhail L. Shur^{a,*}, Philippe R. Spalart^b, Mikhail Kh. Strelets^a^a *New Technologies and Services, 14, Dobrolyubov Ave., St.-Petersburg 197198, Russia*^b *Boeing Commercial Airplanes, PO Box 3707, Seattle, WA 98124, USA*

ARTICLE INFO

Article history:

Accepted 8 February 2011

The peer review of this article was organized by the Guest Editor
Available online 23 March 2011

ABSTRACT

The Large-Eddy Simulation (LES) numerical system established since 2002 for jet-noise computation is first evaluated in terms of recent gains in accuracy with increased computer resources, and is then used to explore the relatively new “microjet” noise-reduction concept (injection of high-pressure microjets in the vicinity of the main jet nozzle exit), which currently attracts attention in the aeroacoustic community. The simulations, which are carried out with an emulation of the microjets by specially designed distributed sources of mass, momentum, and energy in the governing equations, are found to capture the essential features of the flow/turbulence and the far-field noise alteration by the microjets observed in experiments, and to reveal the subtle flow features responsible for the effect of injection on noise. They also confirm the experimental observation that in static conditions microjets provide a noise reduction comparable with that from chevrons in the low-frequency range, and probably have a less pronounced high-frequency penalty. This positive evaluation of the microjets concept is, however, mitigated by the far less favorable results of simulations in flight conditions, which were never studied experimentally. The latter results, which are awaiting an experimental verification, make a practical use of the concept in its current form rather unlikely.

© 2011 Elsevier Ltd. All rights reserved.

1. Introduction

Over the last decade, LES of turbulence coupled with integral acoustic methods, Ffowcs Williams and Hawkings (FWH) or Kirchhoff, has made significant progress and proved to be capable of predicting the far-field noise of turbulent jets in the full Mach number and temperature range of interest in commercial aviation to a very useful degree (see, e.g., [1–4]). This justifies the use of such numerical systems to evaluate the performance of jet-noise-reduction devices, which is the most important application area for non-empirical methods of jet-noise prediction. Of course, LES alone still cannot resolve all the related issues, first of all, because of the insufficient frequency range and the inability to capture the excessively complex geometry of full industrial cases with pylons, heat shield, vents, etc., with high-order structured CFD codes. These have proven to be most successful in jets aeroacoustics. However, unlike flow measurements, LES provides the entire flow and sound fields thus greatly supporting the design efforts. It also sets no limits to the ambient flow velocity, in contrast

[☆] This article is an expanded, peer-reviewed version of an article previously published in *Procedia Engineering* 6C (2010) 44–53.

* Corresponding author. Tel.: +7 812 329 4792; fax: +7 812 329 4791.

E-mail address: mshur@cfdsu.spbstu.ru (M.L. Shur).

with most experimental facilities. An example of numerical system for jet noise prediction supporting the high potential of the LES-based approaches is given in [5–7]. This system established since 2002, has now reached a good level of confidence over a wide range of geometries and flow conditions. Owing to improvements made both to the turbulence simulation and the far-field extrapolation [6,7], geometries now include dual nozzles, with stagger and with an external core plug; noise-reduction devices such as chevrons and bevels are also routinely treated. This is made possible by a two-stage simulation procedure which includes a coupled nozzle/jet plume RANS computation, in the first stage, and Implicit LES (i.e., without activation of the SGS model) of the jet plume alone, in the second stage. Note that in this stage the inflow velocity profiles are imposed from the already available RANS solution, and no time-dependent velocity perturbations are introduced (a more detailed discussion of the two-stage approach is given in [6]). The approach has proven to reproduce the effect of the internal nozzle geometry and maintain realistic boundary layers without the extreme cost of a coupled nozzle–plume LES [8]. Combined with low-dissipation high-order numerics, this ensures a rapid transition to turbulence in the jets shear layer, which is of crucial importance for an accurate noise prediction.

The paper presents a new application of the system [5–7] to the evaluation of noise-reduction devices, namely, of the placement of microjets around the main jet, an idea currently attracting significant attention in both experimental and CFD jet-noise communities as an alternative or a complement to chevron nozzles. This is preceded by a discussion of recent results of simulations of the simple subsonic $M=0.9$ jet carried out on much finer grids than those used in our earlier studies [5,9]. These give an idea of the accuracy increase possible with increasing computer power.

2. Grid-sensitivity study of LES-based noise prediction for $M=0.9$ round jet

A classic $M=0.9$ unheated jet is considered, which was analyzed in numerous LES-based jet noise studies including those of the authors [5,9]. The jet is that from a conical nozzle studied experimentally by Viswanathan [10]. The Reynolds number based on the exit diameter $D=0.06223$ m is equal to 1.1×10^6 , and according to a RANS computation inside the nozzle, the nozzle-exit boundary layer thickness and the momentum thickness are $8 \times 10^{-3}D$ and $5 \times 10^{-4}D$, respectively. In the present work, two new simulations of this jet are carried out on much finer grids than those used in [5,9]. Table 1 summarizes the major characteristics of both “old” and “new” grids (all dimensions are normalized with D).

All four grids have the same topology with two overlapping blocks [5], the inner one Cartesian, and the outer one cylindrical. The computational domain extents from $10D$ upstream to $70D$ downstream of the nozzle exit. In the radial direction the outer radius of the domain varies from $15D$ in the vicinity of the nozzle to $30D$ at the end of the domain. For the far-field noise extraction, a set of nested closed funnel-shaped control FWH surfaces is used, with the narrowest surface placed in immediate vicinity of the turbulent area. Based on the value of Δr at the FWH surface and assuming that 8 cells per wave length are sufficient for an accurate representation of sound propagation from source region up to the control surfaces, the estimates of the highest Strouhal number resolved by the grids are around $St=2.5$ for Grid 1, $St=7$ for Grids 2 and 3, and $St=12$ for Grid 4. Note that Grid 3 differs from Grid 2 only by the doubled number of nodes in the azimuthal direction, whereas in Grid 4 the steps in all the three spatial directions in the “sensitive” flow area are reduced by a factor of about 1.5 compared to Grid 3.

Before discussing the results we briefly describe the procedures used for computing turbulence statistics and noise spectra. In all the simulations, the accumulation of unsteady information needed for both was started after a transient period of 500–600 convective time units, D/U_{jet} , and lasted for around $250D/U_{jet}$. As discussed in detail in [5], the narrow-band spectra in all our simulations contain a spurious tone in the high frequency range associated with the shear layer roll-up (the tone frequency depends on the grid used and increases with grid refinement). So, in order to avoid aliasing errors in the computed noise spectra, the time interval between the samples saved for the FWH acoustic post-processing was adjusted to resolve the tone frequency, and was typically equal to 3–4 time-steps of integration of the governing equations (given in Table 1). The narrow band noise spectra were computed with the use of the entire time sample and 10-percent cosine taper (so called Tukey) windowing [11] of the time-signals before entering the Fourier transform, followed by the energy-conserving correction. Note, finally, that when integrating the spectra to obtain OASPL, frequencies higher than that of the spurious tone were discarded.

Table 1
Major parameters of grids.

	Grid 1 (used in [5])	Grid 2 (used in [9])	Grid 3 (present work)	Grid 4 (present work)
Outer block size $N_x \times N_r \times N_\phi$	$308 \times 81 \times 64$	$515 \times 101 \times 80$	$515 \times 101 \times 160$	$601 \times 158 \times 240$
Total cells count	1.6 M	4.2 M	8.4 M	23 M
Δx at nozzle exit	0.011	0.008	0.008	0.005
Average Δx for $0 < x < 4$	0.033	0.022	0.022	0.016
Average Δx for $4 < x < 10$	0.11	0.055	0.055	0.042
Min Δr in shear layer	0.003	0.0025	0.0025	0.0018
$r\Delta\phi$ in shear layer	0.05	0.04	0.02	0.013
Time step, $\Delta t U_{jet}/D$	0.02	0.01	0.006	0.004

Results of the simulations are presented in Figs. 1–5. In particular, Fig. 1 gives an idea of the turbulent structure of the jet from the simulation on the finest grid (Grid 4). In line with our previous results obtained on coarser grids, it shows that without any resolved inflow turbulence, a rapid spontaneous transition does occur and no regular (Kelvin–Helmholtz like) structures are formed in the initial part of the jet shear layer. This is visibly displayed also in Fig. 2, where the distributions

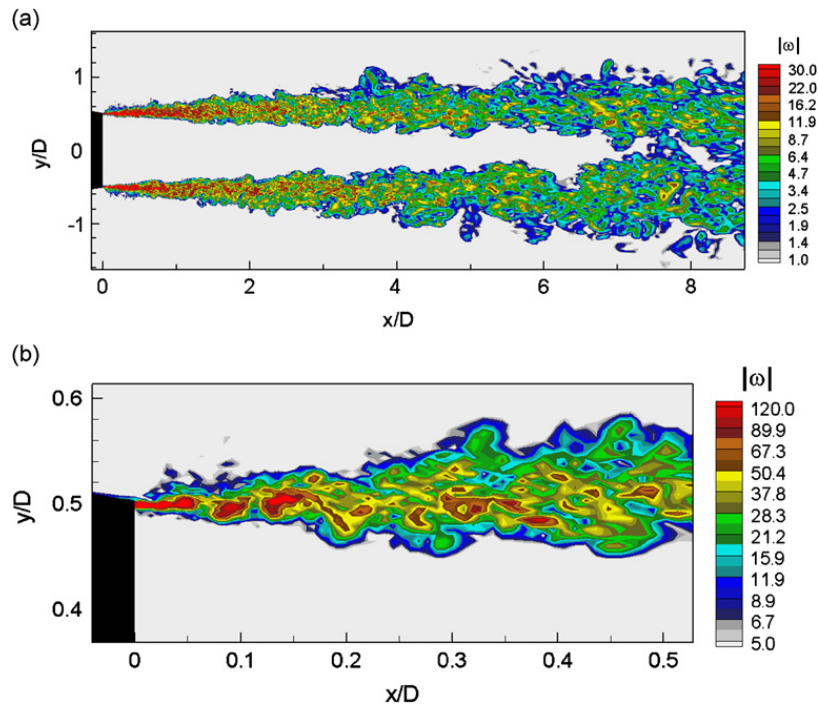


Fig. 1. Snapshot of vorticity magnitude in the $M=0.9$ jet from simulation on Grid 4 from Table 1 (a) and its zoomed fragment in the vicinity of nozzle edge (b).

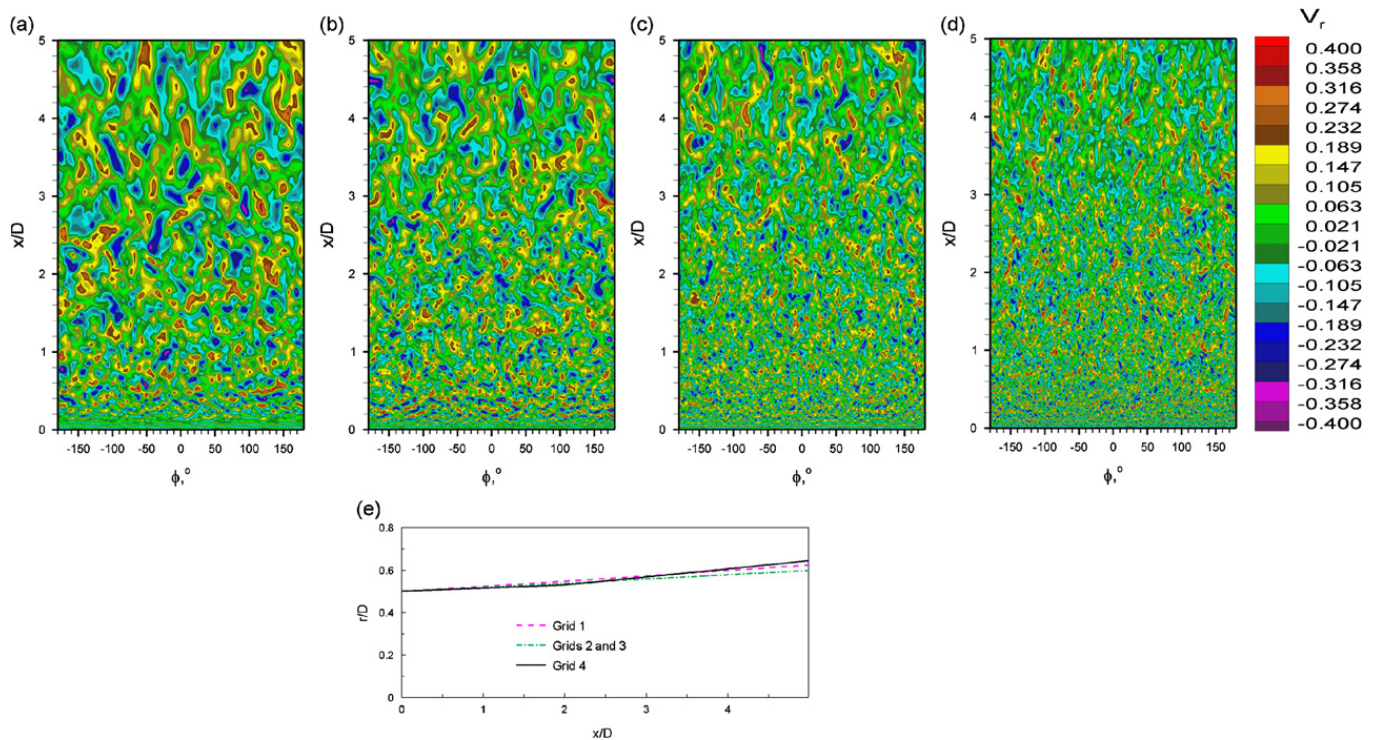


Fig. 2. Instantaneous radial velocity in $M=0.9$ jet on a grid surface inside the mixing layer from simulations on different grids: (a) Grid 1, (b) Grid 2, (c) Grid 3, (d) Grid 4, and (e) radial position of the surface.

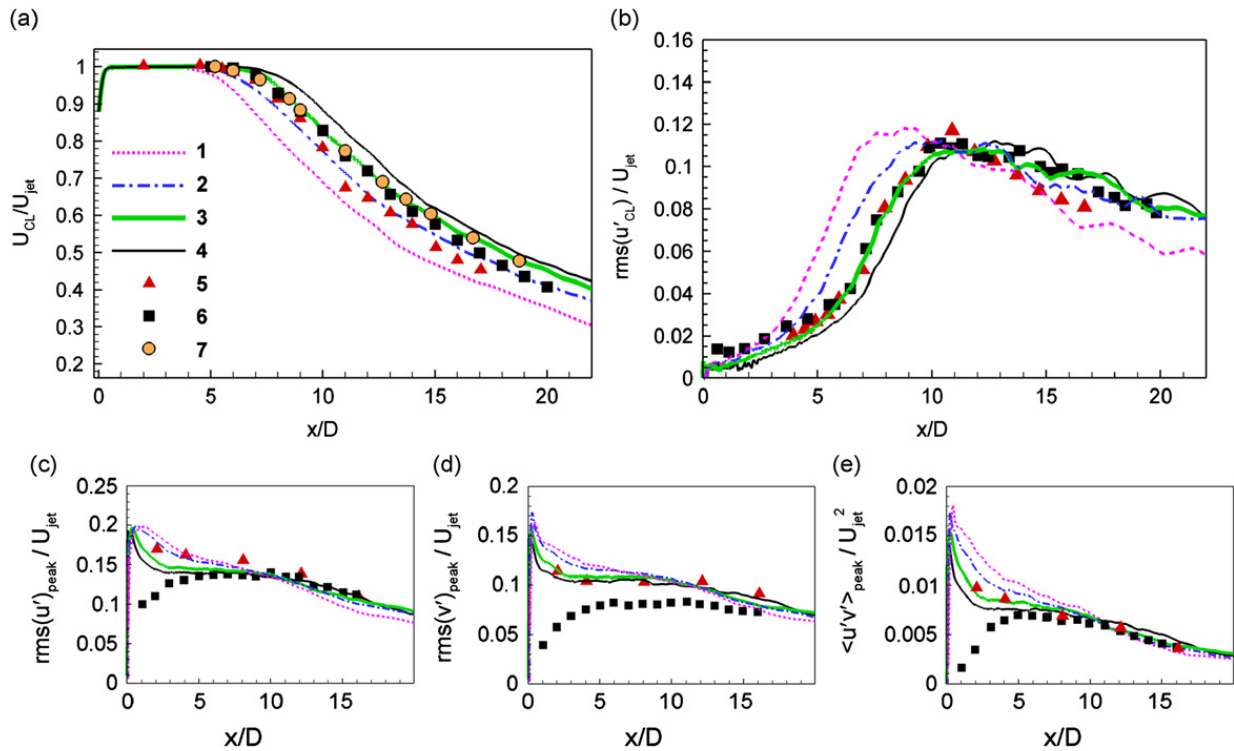


Fig. 3. Centerline distributions of mean velocity (a) and its rms (b) and streamwise distributions of peak Reynolds stresses (c)–(e) in $M=0.9$ jet from simulations on different grids. 1–4: LES, Grids 1–4, respectively; 5: data [12,13] (LDV, hot wire), 6: data [14] (PIV), and 7: data [15] (PIV).

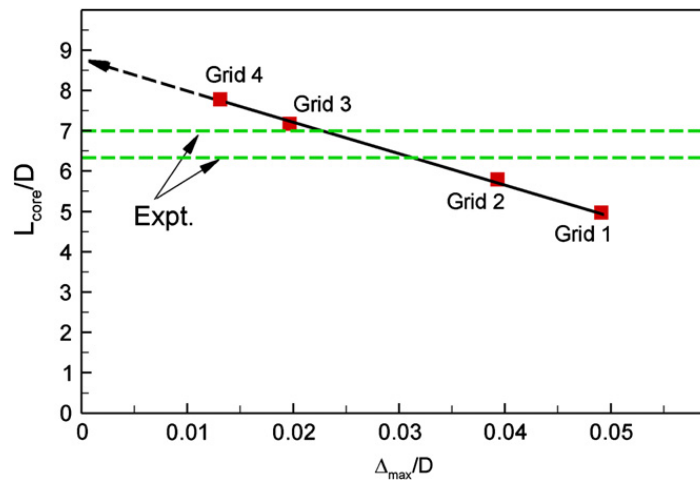


Fig. 4. Effect of grid refinement on predicted length of potential core. Δ_{max} is the grid-step size in the initial ($x < 3D$) jet region; the core length is defined as distance from nozzle exit plane to a point where centerline mean streamwise velocity becomes equal to $0.98U_{jet}$.

are presented of the radial velocity in the mixing layer (with the x and ϕ axes adjusted to give a ratio of 1 between x and $r\phi$), obtained in the simulations on all four grids. The figure demonstrates the rapid three-dimensionalization of the layer, quite natural at the considered high Reynolds number and with a thin boundary layer at the nozzle exit. Note also, that as could be expected, the transition to turbulence is grid-dependent (it starts earlier with a finer grid).

Fig. 3 demonstrates the effect of grid on major mean and statistical aerodynamic characteristics of the jet. It shows that, although grid-independence is not reached uniformly, a trend to convergence is observed, especially considering that the difference between the Grids 3 and 4 is 1.5 times larger than that between the Grids 2 and 3. In terms of agreement of the predictions with the data, overall it improves, but the finest grid results in some overestimation of the length of the potential core compared to experiments. Based on Fig. 4, it is natural to expect this trend to continue with further grid refinement, and in the “infinite grid limit” the potential core might be as long as almost $9D$. Note that a similar overestimation of the length of the jet potential core has been observed by Uzun and Hussaini with very fine grids [8]. As of today, the reasons of this deficiency are not clear. One conjecture is that it is caused by the use of ILES. Another is that the feedback loop between jet turbulence and nozzle is not reproduced accurately enough by the system of boundary

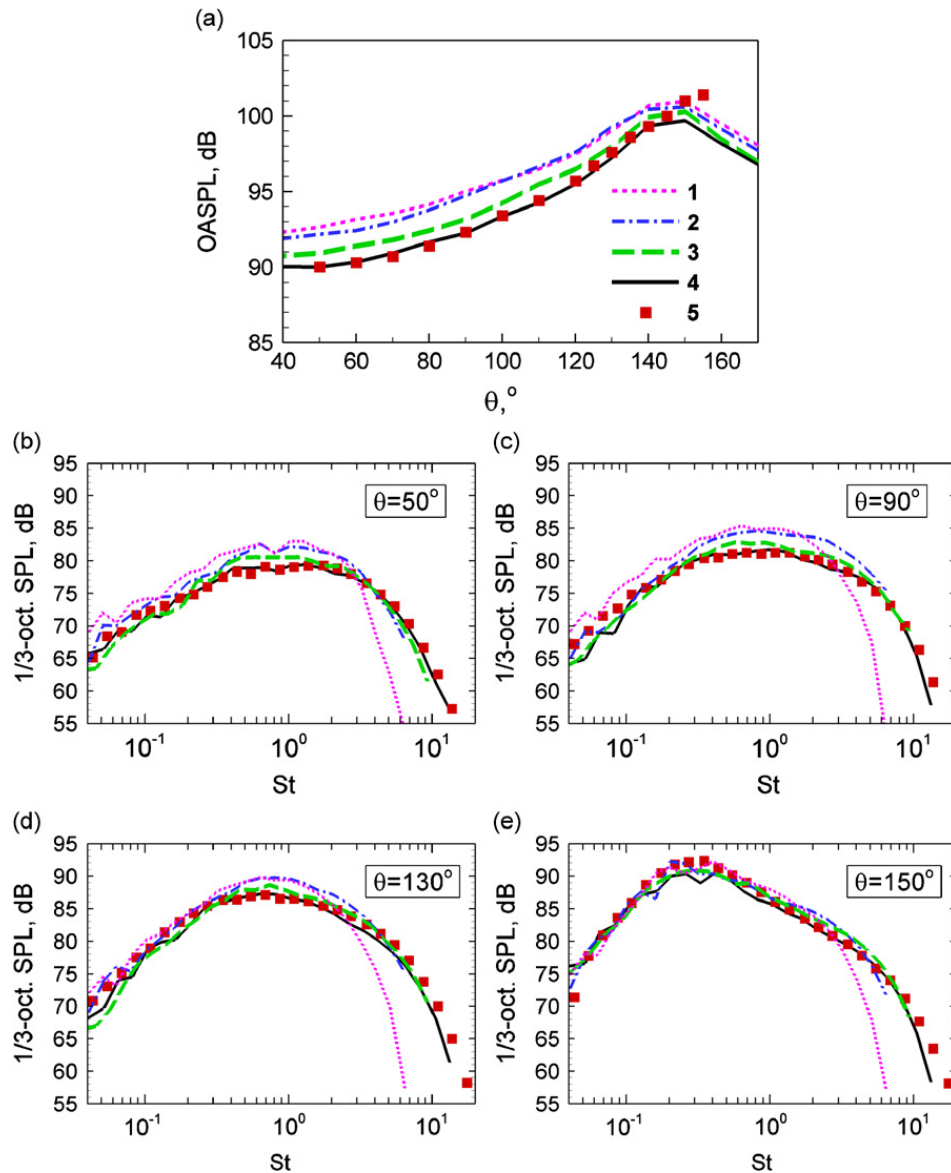


Fig. 5. Overall noise directivity (a) and 1/3-octave spectra at different observer angles (b)–(e) for $M=0.9$ jet from simulations on different grids. Distance $98D$. 1–4: LES, Grids 1–4, respectively; 5: experimental data [10].

conditions used. Uzun and Hussaini included the nozzle in their simulations, but we presume that, for instance, the mass flow was not allowed to fluctuate. Such fluctuations could drive the shear-layer instability, and depend on the geometry much farther upstream than simulations have reached.

As far as the Reynolds stresses are concerned, although uniformly reliable experimental measurements in the early part of the mixing layer ($x/D < 2$) are not available (PIV measurements are known to significantly underestimate the stresses because of insufficient spatial resolution), all the simulations seem to suffer from an overshoot of resolved stresses in this region, and grid refinement leads mostly to narrowing of the overshoot extent. Other than that, on Grids 3 and 4, the peak values of the stresses in the shear layer are showing signs of a self-similar state with flat behavior up to $x/D \approx 10$.

Moving on to the results of the far-field noise computations presented in Fig. 5, it should be noted, first of all, that the trend to grid convergence in the noise predictions is more definitely pronounced, and that grid refinement results in a distinct improvement of agreement with measurements not only in the high-frequency range, as expected, but also with respect to the spectral maxima at a Strouhal number near 1.0 for all the observer angles less than 140° . For the highest resolved frequency, on the finest grid (Grid 4) the upper limit of reliable prediction is as high as $St \approx 12$ (for the one-third octave band) compared to $St \approx 2$ on the coarsest grid (Grid 1).¹ This is already not crucially far from the practically meaningful range of $St=15-20$.

¹ The high-frequency ends of the spectra presented in Fig. 5 correspond to the last 1/3-octave bands not containing the high-frequency spurious tones mentioned above.

Note that resolution of the jet-generated noise up to similar Strouhal numbers ($St=15$ in the narrow-band spectra) was reached in an elaborate simulation of the jet from a chevron nozzle by Uzun and Hussaini [8], for the observer at a polar angle 90° . That simulation was carried out in the framework of a complete LES of part of the nozzle and the initial part of the jet plume (up to $x/D=10$) on a grid with 400 million cells; our Grid 4 has 23 million. The simulation includes LES content in the nozzle boundary layer. In principle, this approach is capable of providing a realistic turbulent content at the nozzle exit and, therefore, a physically correct representation of the rapid transition to turbulence typical of the high Reynolds number jet shear layers. However, according to their own estimates [16], the grid needed to achieve this is huge (more than 40 billion cells). For this reason the authors of [8] have been forced to decrease the Reynolds number in the simulation by a factor of 12 from the experimental value of 1.2×10^6 . Although this evidently causes a crucial alteration of the boundary layer turbulence, especially in the buffer layer, as mentioned, the approach does not prevent the accurate prediction of the noise spectra in the jet-normal direction up to $St=15$. This, in fact, suggests that in terms of noise prediction the accurate representation of the nozzle-exit boundary layer and, particularly, its turbulence content is not crucial, provided the inaccuracy does not cause a significant delay of the transition to turbulence in the jet shear layer. This is also strongly suggested by the present study where quite a similar accuracy in noise prediction to that in [8] is reached on a much coarser grid without any LES content in the incoming boundary layer. Recall that both codes implement high-order differencing; conversely the FWH implementations and details of the FWH surfaces can have a significant impact on noise predictions. Thus for the practically meaningful range of Reynolds numbers and frequencies, the approach based on the complete nozzle-plume LES of the jets appears to be computationally extremely expensive, without a clear improvement in noise results.

Coming back to Fig. 5, it should be noted that the largest disagreement with experiment resides at high θ angles, but the considerable change in the spectral shape at $\theta > 130^\circ$ is not missed by the simulation. For instance, at $St=0.3$, the experimental acoustic energy rises between 130° and 150° by a factor 4.5, while the numerical result rises by only about a factor 3. The sound level is somewhat insufficient, but the shape change is physically encouraging.

One more important conclusion based on the results presented in Fig. 5 is that even with grids that are quite affordable nowadays in routine computations (Grid 2 from Table 1), the numerical system [5–7] ensures a fairly accurate representation of the jet noise up to St around 5. This allows using such modest grids for the evaluation of different jet-noise-reduction devices without the risk of missing a “high-frequency penalty” typical of noise-reduction concepts (the “crossover” frequency for all the known concepts being well below $St=5$). Several examples of such applications are presented in [6,17], where we have considered chevron nozzles, dual nozzles with fan-flow deflecting vanes, and single and dual beveled nozzles. Below we present one more such example, namely, the evaluation of the microjet noise-reduction concept.

3. Evaluation of microjet noise-reduction concept

3.1. Introduction

As mentioned, this concept currently attracts attention as a potential alternative to chevron nozzles, with the advantage of activating the control system only when it is needed (e.g., take-off/landing flight stages), thus avoiding the thrust loss in cruise which is typical of chevrons. A positive effect of microjets (MJ) on the noise was first reported for supersonic and sonic jets with shocks (see e.g., [18,19]). For subsonic jets, experimental investigations of the effect of MJ are mostly restricted to the classic $M=0.9$ unheated jet [14,20,21]. They show that for this jet MJ-injection results in a noise reduction of 0.5–2 dB, depending on the MJ parameters and the observer angle, and in shifting of the high-frequency noise penalty observed for chevron nozzles to significantly higher frequencies (and, therefore, to lower noise amplitudes). Similar conclusions were drawn based on the experiments for a lower Mach number ($M=0.3$) jet carried out with a little different MJ design [22]. The studies have also indicated a mechanism for the noise reduction caused by MJ. In particular, detailed PIV measurements of the flow and turbulence characteristics carried out in [14,20] for the classical configurations with 18 and 8 MJ, respectively, have shown that MJ-injection into the main jet leads to a formation of streamwise vortices which suppress turbulent fluctuations in jet's shear layer.

LES-based studies of MJ available in the literature are rather limited [22–25]. Their major finding is that LES is capable of capturing the effect of MJ on both aerodynamics and jet noise observed in the experiments. In particular, simulations do predict a 1–2 dB low frequency noise-reduction which is close to the experimental observations. However, even the most complete study with gridding of the MJ [25] (124 million cells total), does not claim to resolve medium- or high-frequency ($St > 3$) noise and, therefore, does not allow the high frequency noise penalty issue to be addressed. Other than that, neither numerical nor experimental studies consider the performance of the device in flight conditions, even at relatively low speeds after take-off, which is crucial for an assessment of the practical value of the concept. For this reason, the present work focuses on the analysis of exactly these insufficiently studied aspects of the microjets, i.e., on their effect in flight conditions and on the evaluation of the high-frequency noise penalty.

3.2. Description of simulations

The simulations are carried out for the system studied in the experiments of Alkislar et al. [20], which includes 8 equally spaced MJ injected into $M=0.9$ unheated main jet (see Fig. 6). Similarly to other LES studies [23,24], the MJ are not

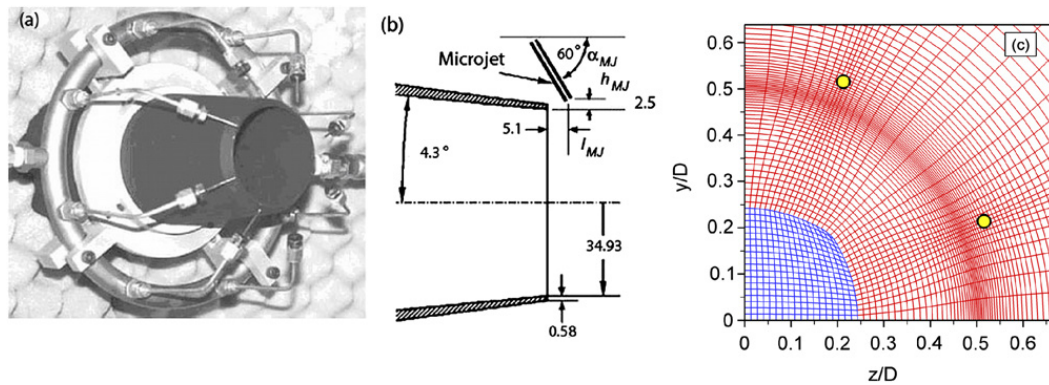


Fig. 6. Configuration tested by Alkislar et al. [20] (a, b) and fragment of LES-grid in YZ -plane in the microjet injection cross section (c). Dimensions are in mm. Circles in frame (c) show regions with non-zero source terms in the governing equations emulating microjets.

gridded but “created” by means of source terms in the governing equations. However, in contrast to these studies, the sources are not confined to only one computational cell but are distributed in space, with appropriate grid clustering in the vicinity of the injection ports (the specific form of the source terms is presented in the Appendix). This approach ensures a fair representation of the microjets’ size and local characteristics, although with the present grids, there is no claim to an accurate reproduction of their “internal” turbulence.

In addition to the two simulations (baseline and with MJ) corresponding to the static conditions studied in the experiments [20], two similar simulations are carried out for flight conditions, at external flow Mach number $M_{CF} = 0.2$, as is typical of take-off/landing regimes. The parameters defining the microjets’ size and position (see Fig. 6) were the same as in [20]: $d_{MJ} = 8 \times 10^{-4}$ m, $\alpha_{MJ} = 60^\circ$, $l_{MJ} = 0.0051$ m, $h_{MJ} = 0.0025$ m. The diameter of the main jet is $D = 0.06985$ m. The total (through all the 8 MJ) mass flow rate was 4 g/s ($\approx 0.3\%$ of the main jet mass flow rate) which corresponds to fully expanded Mach number of 1.5.

The grid used in all the simulations is similar to Grid 2 for the round jet of the previous section (see Table 1). However, in order to ensure a more accurate representation of the MJ, it is refined in the azimuthal direction in the vicinity of the MJ as shown in the right frame of Fig. 6. This non-uniformity is smoothly eliminated as the distance from the MJ injection region increases. The r -step of the grid is also slightly refined near the radial location of the injection ports. In total, the grid has around 7.6 million cells, with 144 cells in the azimuthal direction.

3.3. Results and discussion

Figs. 7–14 illustrate the effect of the microjets on the aerodynamics and turbulent structure of the main jet in static and flight conditions. They reveal two major trends which help to explain the effect of MJ on noise.

Fig. 7, where an isosurface is plotted of the velocity magnitude $|\mathbf{U}| = 0.5U_{jet}$, visibly displays an intensification of fine-grained turbulence in the immediate vicinity of the MJ injection into the main jet stream and further downstream. This effect is clearly pronounced both in static and flight conditions as demonstrated by Fig. 8, which shows snapshots of the magnitude of vorticity in the meridian jet section passing through the center of a microjet for all the four considered jets. Note that exactly this behavior is probably the reason of the high-frequency noise penalty caused by MJ (see below).

In contrast to this, the large-scale turbulence activity in the shear layer of the main jet becomes weaker with MJ injection, and its damping is crucially different for the jets in still air and in flight. These trends are qualitatively illustrated by Fig. 9, which shows the instantaneous radial velocity fields for the four jets, and by Fig. 10 presenting instantaneous isosurfaces of the λ_2 -criterion (second eigenvalue of the velocity gradient tensor) which visualizes vortical structures. The figures suggest that in static conditions, the large-scale turbulence in the shear layer is tangibly suppressed in the controlled case. However, in flight conditions this effect appears to be very weak, compared to a similar effect caused by the flight itself. This is supported quantitatively by Figs. 11 and 12, which compare the turbulence energy spectra and fields of turbulent kinetic energy (for developed turbulence, this quantity is known to be dominated by large-scale velocity fluctuations). Note that a decrease of the turbulent kinetic energy in the shear layer of the controlled jet in still air is quite consistent with experimental observations [14,20].

Fig. 13 presents the streamwise distributions of the peak values of Reynolds stresses for all the cases. It shows that in the initial part of the shear layer ($x/D < \sim 0.8$), the injection causes a significant increase of the stresses both in the static and flight conditions, whereas farther downstream the peak stresses in the controlled jets are lower than those in the baseline ones, the effect being much more pronounced in the static case. This is consistent with the influence of MJ injection on the small- and large-scale turbulence discussed above. Note, finally, that a decrease of the peak stresses in the

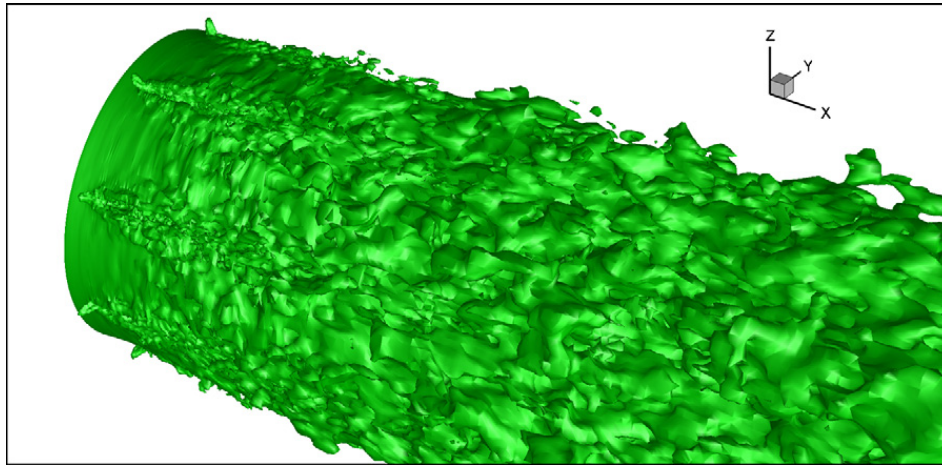


Fig. 7. Isosurface $|\mathbf{U}|=0.5U_{jet}$ from LES of controlled jet in static conditions.

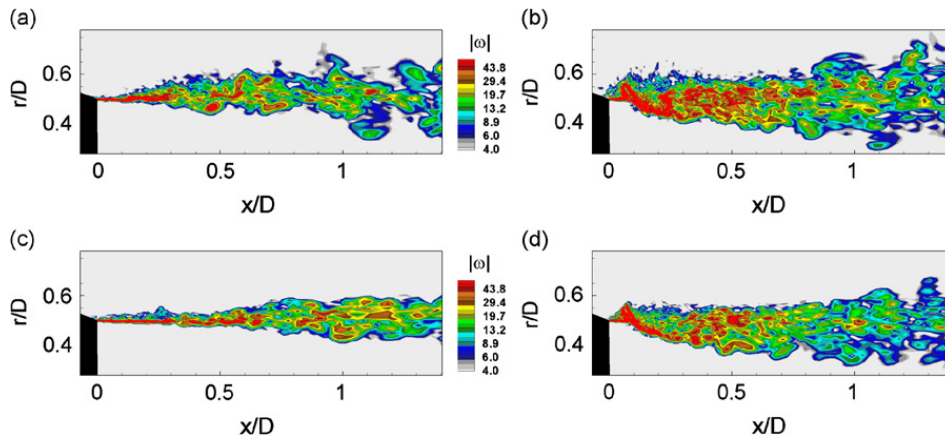


Fig. 8. Instantaneous fields of vorticity magnitude in meridional section passing through microjet center: (a) baseline (no MJ injection) jet in still air, (b) controlled jet in still air, (c) baseline jet in flight, and (d) controlled jet in flight.

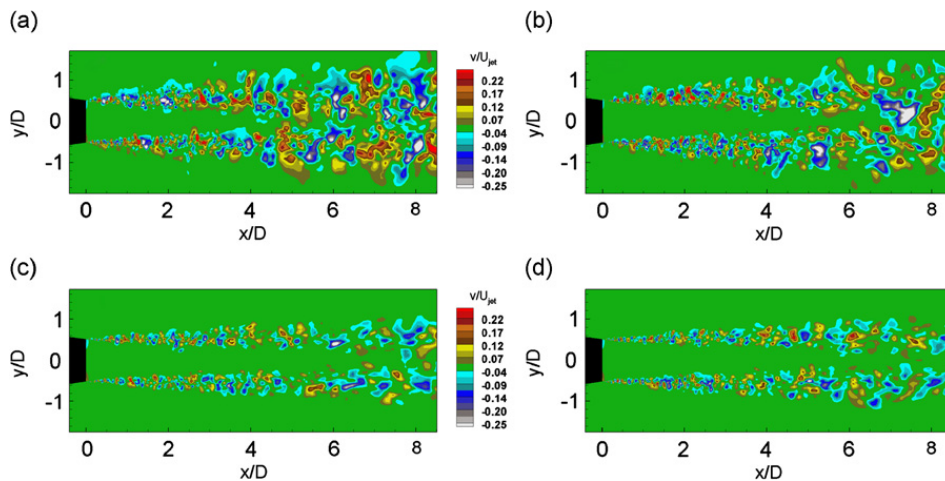


Fig. 9. Instantaneous fields of radial velocity in meridional plane between microjets: (a) baseline jet in still air, (b) controlled jet in still air, (c) baseline jet in flight, and (d) controlled jet in flight.

controlled static jet takes place only up to the distance of about twice the length of the jet potential core. Qualitatively, this behavior, again, agrees with the experiment [20].

Finally, Fig. 14 shows the predicted alteration of the centerline distributions of the mean velocity and TKE caused by the MJ. The figure suggests that in line with the experiments for the static jets and consistently with the trends we just described, the injection results in quite a noticeable elongation (by around one diameter) of the jet's potential core and

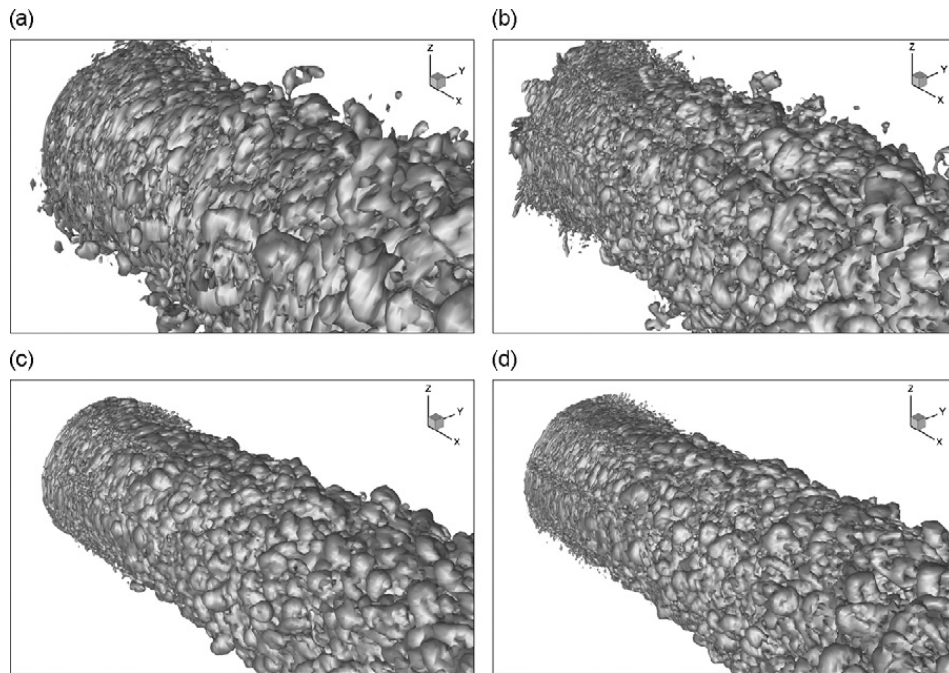


Fig. 10. Instantaneous isosurface $\lambda_2=0.2 U_{jet}/D$ from four simulations: (a) baseline jet in still air, (b) controlled jet in still air, (c) baseline jet in flight, and (d) controlled jet in flight.

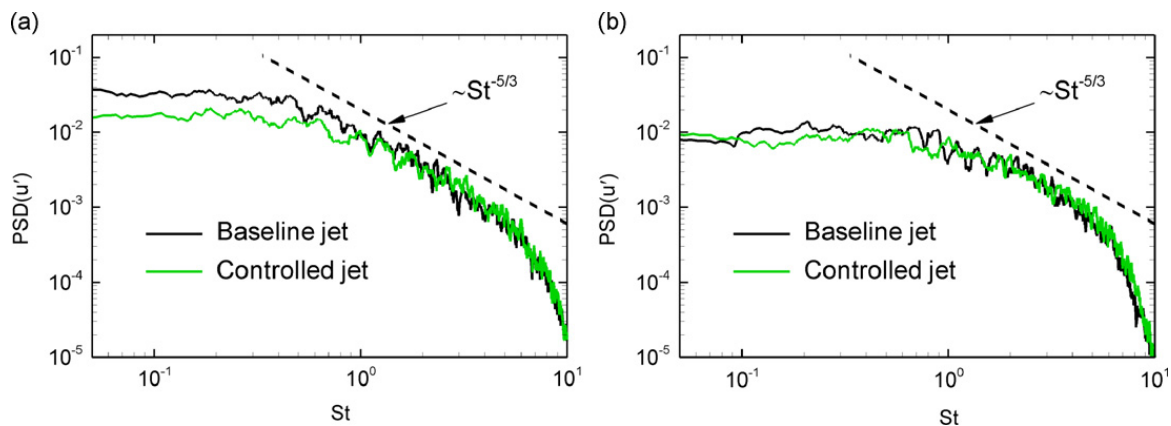


Fig. 11. Power spectral density of streamwise velocity fluctuations at point $(x, r)=(2.0D, 0.5D)$ in meridian plane between microjets: (a) jets in still air and (b) jets in flight.

decrease of the maximum centerline TKE, whereas in flight conditions, the centerline distributions are virtually insensitive to the MJ injection.

We now discuss the results of computations of major noise characteristics with and without MJ in static and flight conditions, presented in Figs. 15–17. In general, all the trends revealed by these figures are consistent with the alteration of the jets' aerodynamics and turbulent characteristics analyzed above.

Fig. 15 provides a visual evidence of the favorable effect of MJ in static conditions, with virtually no effect in flight.

Figs. 16 and 17 summarize the quantitative information on the effect of MJ on the far-field noise.

Two upper rows of Fig. 16 compare the MJ effect on the narrow-band noise spectra obtained in the experiment (Fig. 16a and b) and in the computations (Fig. 16c and d) for static conditions. The numerical results differ from the experiment, by about the same margin as in Fig. 5. One can see that the simulations reproduce the MJ effect fairly accurately. Particularly, exactly as in the experiment, with the MJ, the peaks of the computed spectra at low frequencies ($St=0.2-0.4$) are 1–2 dB lower than for the baseline jet. Also, both in the simulations and experiment, the frequency range of the noise benefit caused by the MJ is rather wide for all the observer angles (only two are shown), and at large frequencies some noise penalty is observed. Moreover, the predicted crossover frequency, in agreement with the measured one, is around $St=3$. Note that the noise amplitude at this frequency is already strongly reduced relative to peak levels, and so the high-frequency penalty of the MJ has almost no effect on the integral noise (in practice, the different weightings used in noise certification may alter this tendency). Recall that for chevron

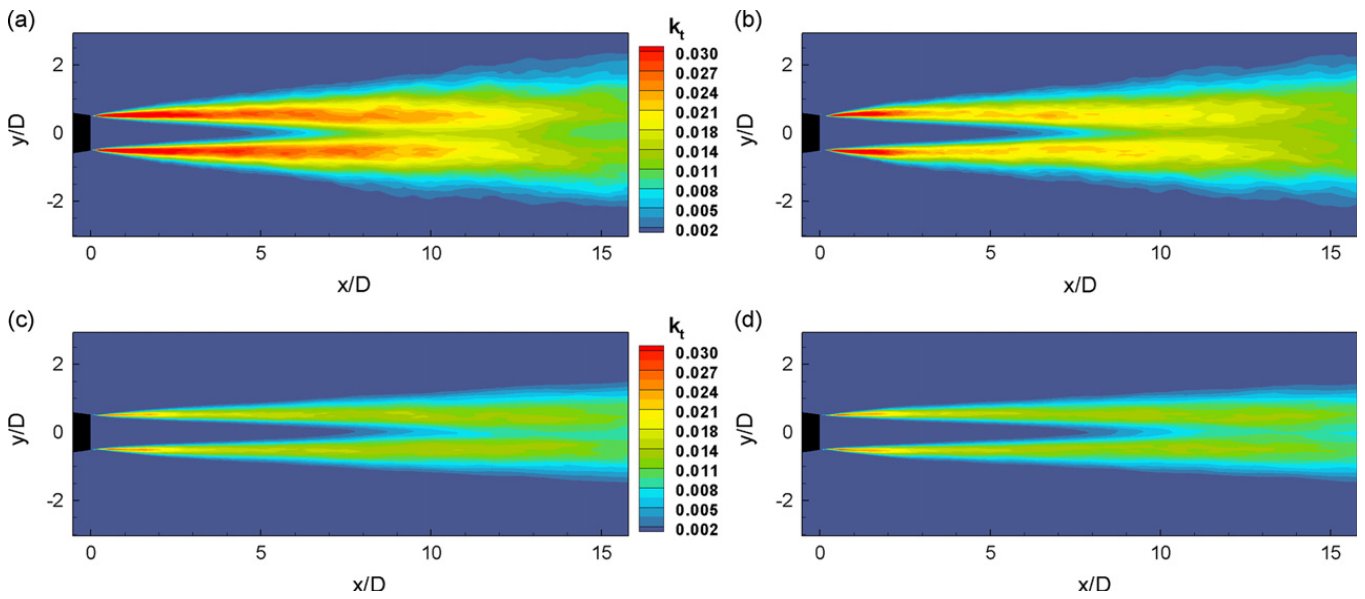


Fig. 12. TKE fields in meridian plane between microjets: (a) baseline jet in still air, (b) controlled jet in still air, (c) baseline jet in flight, and (d) controlled jet in flight.

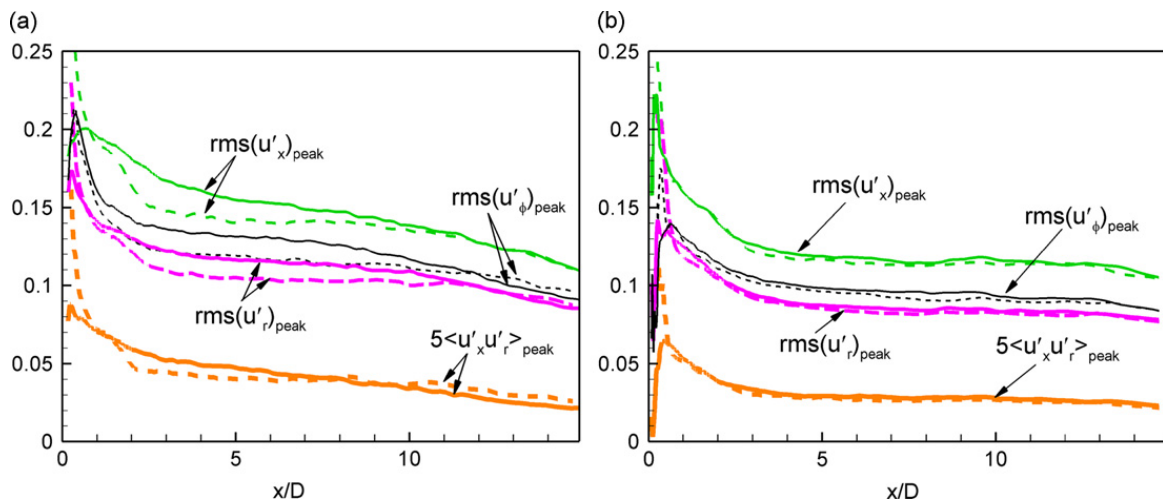


Fig. 13. Effect of MJ-injection on streamwise distributions of peak Reynolds stresses (a) jets in still air and (b) jets in flight; solid lines: baseline jets; dashed lines: controlled jets.

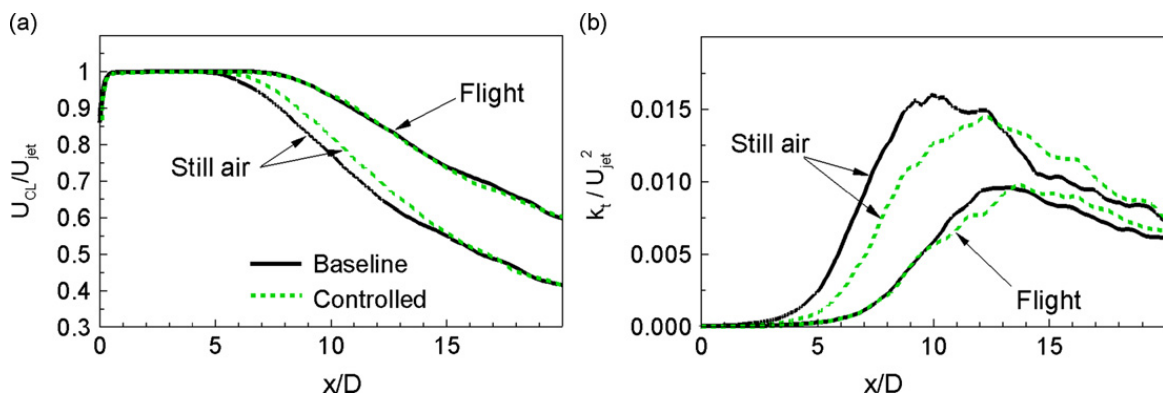


Fig. 14. Centerline distributions of mean velocity (a) and TKE (b) in baseline and controlled jets in still air and flight.

nozzles the crossover frequency can be significantly lower ($St=1-1.5$, depending on the observer angle), resulting in an increase of the integral noise at close to jet-normal observer angles. Thus, results of the computations support the experimental finding [20] that in this sense MJ injection in static conditions can be more beneficial than chevrons.

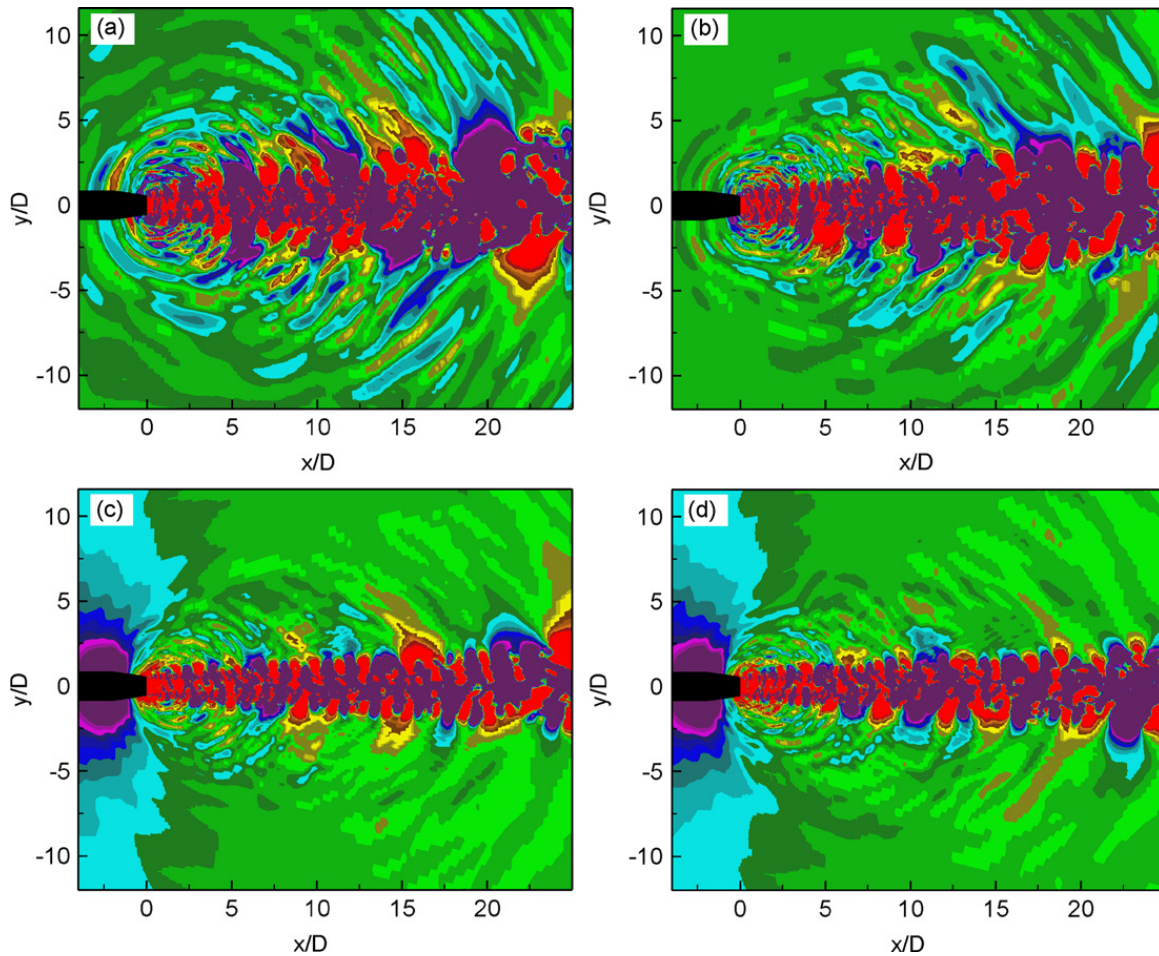


Fig. 15. Instantaneous pressure contours in the acoustic range $-0.001 < (p/p_0 - 1) < 0.001$: (a) baseline jet in still air, (b) controlled jet in still air, (c) baseline jet in flight, and (d) controlled jet in flight.

A strong difference of the effect of MJ on the far-field noise in flight and static conditions, which could be expected based on the finding concerning the different effect of MJ on the large-scale turbulent activity of the main jet (see Figs. 9–14), is evident from a comparison of the second and third rows of Fig. 16 (Fig. 16b, c and d, e). One can see that unlike under static conditions, in flight the low-frequency part of the spectra near the spectral peaks is virtually unaffected by the MJ injection (the difference between the baseline and controlled cases is within ~ 0.5 dB, i.e., does not exceed the accuracy our simulations can claim). At the same time, the high-frequency noise penalty for the controlled jet is of the same order as that for the jet in still air, and the crossover frequencies in flight and in still air are also virtually the same ($St \approx 3$).

As for the OASPL directivity of the noise (see Fig. 17), considering that input of the frequencies higher than the crossover one into the integral noise is negligible, it simply reflects the trends discussed above concerning the low-frequency part of the SPL spectra.

Finally, Fig. 18 provides some insight into subtle details of the mechanism of the MJ effect on the main jet turbulence and therefore on the noise. In accordance with the experiment [20], the injection of a microjet results in the formation of a counter-rotating streamwise vortex pair closer to the high-speed side of the shear layer, which first moves in the radial direction towards the jet axis, and then starts moving in the opposite direction (outward in the shear layer). The authors of [20] consider these streamwise vortex pairs as the main reason for the jet turbulence suppression discussed above. An analysis of the LES fields suggests a similar, but not identical scenario of the evolution of the mean streamwise vorticity. As seen in Fig. 18a and b, LES predicts the formation of a more complicated set of vortical structures (effectively two counter-rotating vortex pairs). The inner pair originates from a microjet penetrating inside the main jet and is located close to the high-speed edge of the shear layer. It is intense but dissipates very rapidly (see Fig. 19). The outer pair forms somewhat farther downstream near the jet half-velocity line. Initially it is much less intense than the inner pair, but it decays much more slowly. As a result, at $x \approx 0.8D$ the intensities of the two pairs get close to each other. Further downstream, only the outer pair survives (Fig. 19d) and so probably this pair causes the suppression of turbulence in the shear layer. This interpretation is supported by Fig. 18c, where we present the downstream evolution of the radial coordinates of the centers of the streamwise vortices from the computations and experiment. The figure suggests that the “2-vortex-pair”

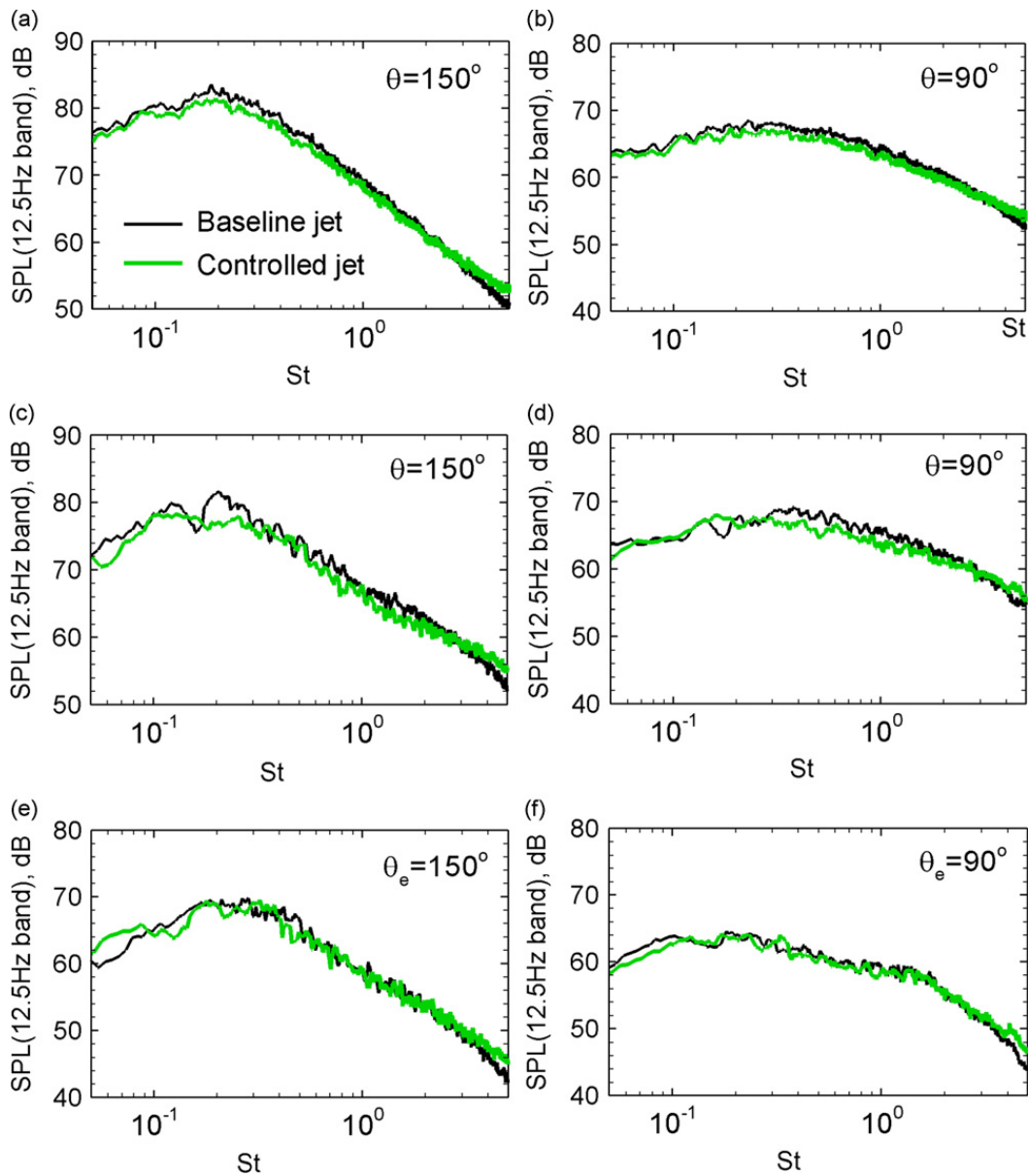


Fig. 16. Measured [20] (a), (b) and predicted (c)–(f) far-field narrow-band noise spectra of baseline and controlled jets at emission distance 100D. (a), (c), (e) emission angle 150°; (b), (d), (f): 90°. (a)–(d): still air; (e), (f) flight.

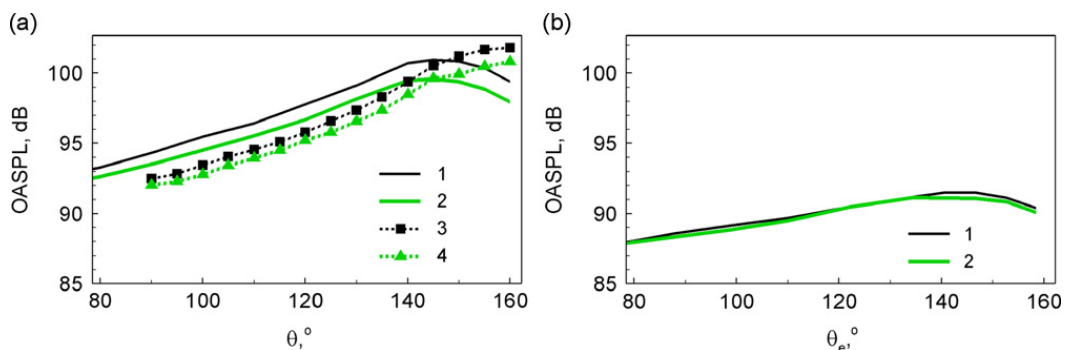


Fig. 17. Measured and predicted far-field noise directivities of baseline and controlled jets: (a) jets in still air, (b) jets in flight; 1, 2: LES, 3, 4: experiment [20]; 1, 3: baseline jets, 2, 4: controlled jets.

scenario, in general, does not contradict the experimental observations and, moreover, allows for an explanation of the non-monotonic evolution of the radial location of the vorticity maximum and the abrupt change of the rate of vorticity decay (not shown) observed in the experiment.

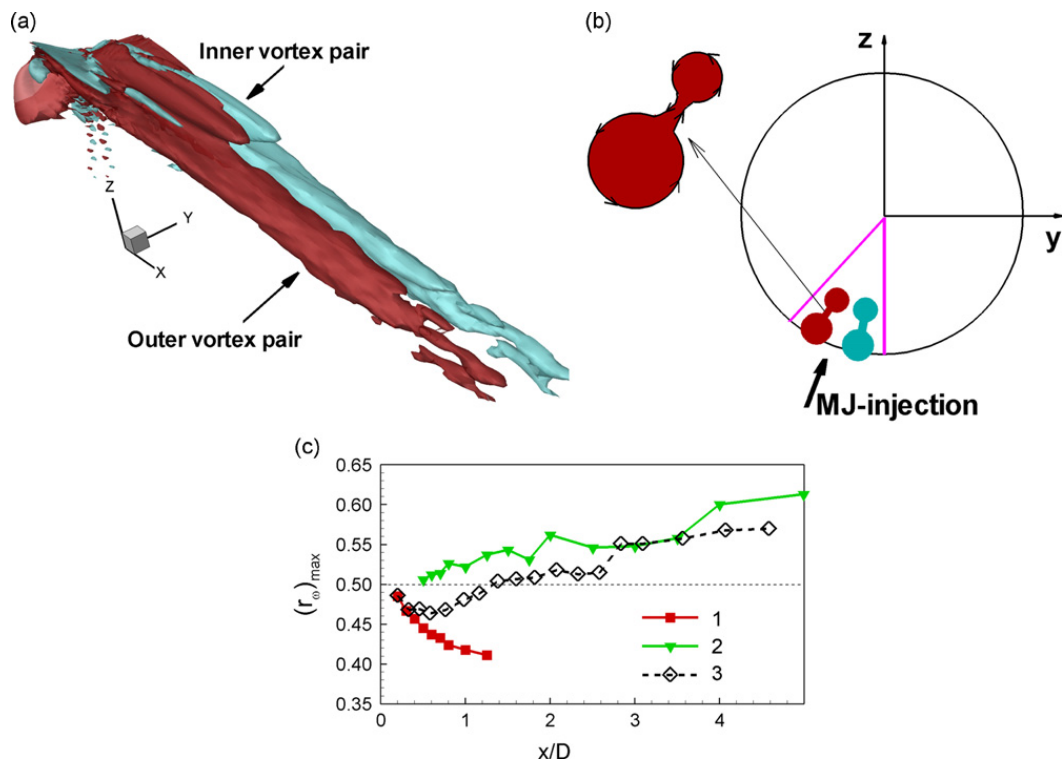


Fig. 18. Isosurfaces of mean streamwise vorticity $\omega_x D/U_{jet} = \pm 0.3$ (a), schematic showing location and shape of the streamwise vortices in YZ-plane (b), and radial coordinates of the vortices centers from LES and experiment (c) for controlled jet in still air. 1: LES, inner vortex; 2: LES, outer vortex; and 3: experiment [20].

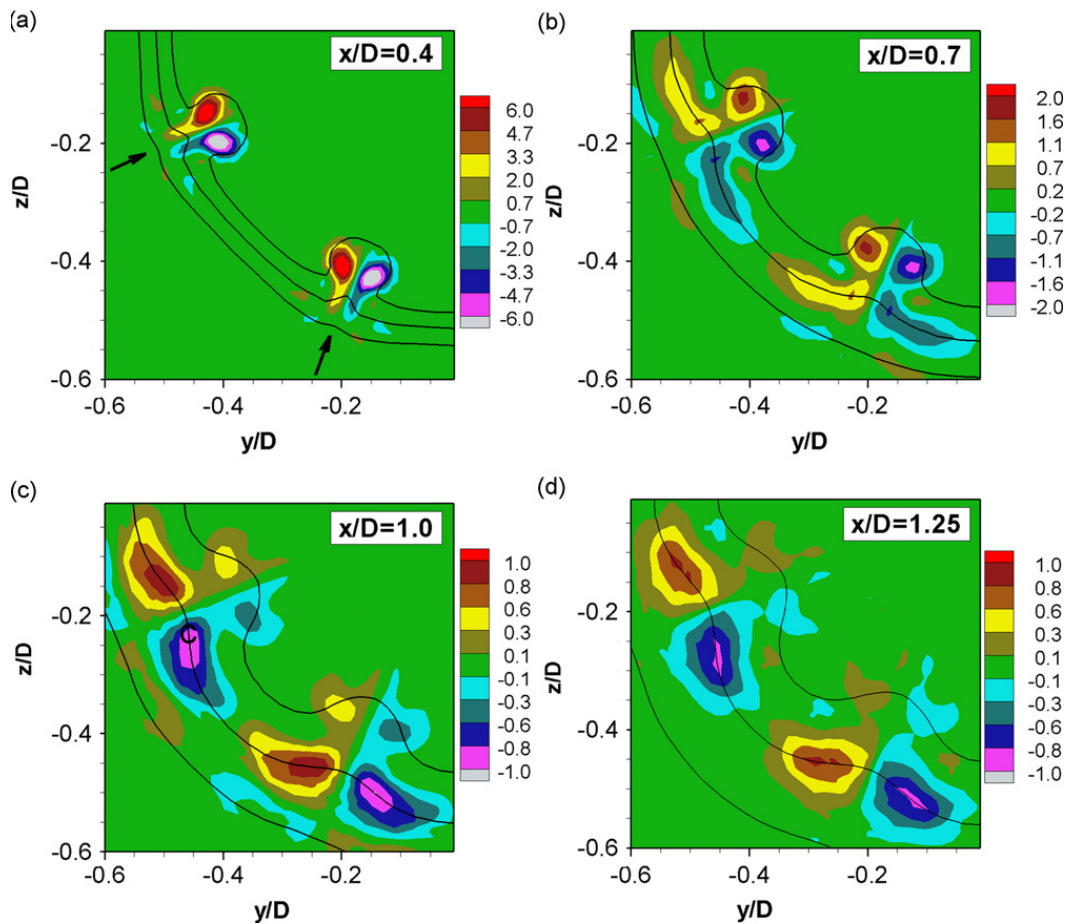


Fig. 19. YZ-cuts of mean streamwise vorticity field $\omega_x D/U_{jet}$ in the initial region of controlled jet in still air. Black lines show mean velocity contours $U/U_{jet} = 0.1, 0.5, \text{ and } 0.9$.

4. Conclusions

LES-based evaluation is carried out of the efficiency of microjet injection for jet-noise suppression in both static and flight conditions. The simulations are performed on a moderately fine grid of about 7.5 million cells, which nonetheless provides resolution sufficient to address the issue of possible high-frequency noise increase caused by the microjets. This capability of the numerical system is demonstrated by a preceding grid-sensitivity study conducted for a simple round jet, of which the results demonstrate a clear trend to grid convergence in LES-based noise prediction and are of significant interest by themselves.

A major outcome of the microjet simulations is that this noise-reduction concept, considered competitive with chevrons nozzles in static conditions, turns out to be virtually “passive” in flight conditions which were never studied experimentally. Specifically, according to CFD, at a typical take-off value of the flight Mach number, the microjet injection does not cause any noticeable reduction of the peak low-frequency noise and still results in the same level of high-frequency noise increase as in static conditions. This finding, which makes a practical use of the concept in its current form rather questionable, is awaiting an experimental verification. Design changes may be tested in the future.

Acknowledgements

This work was funded by Boeing Commercial Airplanes. The authors are grateful to Dr. M. Alkislar for providing experimental data and fruitful discussions.

Appendix A. Source terms emulating microjets

In order to emulate the effect of microjet injection, the following volume source terms are introduced into the right hand side of the governing continuity, momentum, and energy equations:

$$q_\rho(\mathbf{r}) = A_\rho \frac{\Psi(\mathbf{r})}{V_q}, \quad \mathbf{q}_m(\mathbf{r}) = \mathbf{A}_m \frac{\Psi(\mathbf{r})}{V_q}, \quad q_E(\mathbf{r}) = A_E \frac{\Psi(\mathbf{r})}{V_q} \quad (\text{A.1})$$

where $V_q \equiv \iiint \Psi(\mathbf{r}) dx dy dz$ is the “effective” volume of the source and the function $\Psi(\mathbf{r})$ defines its spatial distribution.

This form ensures that, irrespective of the grid used and specific form of $\Psi(\mathbf{r})$, numerical volume integrals of the added sources are equal to the quantities A_ρ , \mathbf{A}_m , and A_E in Eq. (A.1). For the sonic under-expanded microjets considered in the present study, these integrals are assigned based on the fully expanded parameters of the microjets (density $(\rho_{MJ})_{FE}$, velocity vector $(\mathbf{U}_{MJ})_{FE}$ parallel to the microjets direction, temperature $(T_{MJ})_{FE}$, and pressure $(p_{MJ})_{FE} = p_0$) as follows:

$$\begin{aligned} A_\rho &= (\rho_{MJ})_{FE} (|\mathbf{U}_{MJ}|)_{FE} (S_{MJ})_{FE}, \\ \mathbf{A}_m &= A_\rho (\mathbf{U}_{MJ})_{FE}, \\ A_E &= A_\rho [c_V (T_{MJ})_{FE} + (|\mathbf{U}_{MJ}|)_{FE}^2 / 2 + p_0 / (\rho_{MJ})_{FE}] \end{aligned} \quad (\text{A.2})$$

where c_V is the specific heat capacity at constant volume and $(S_{MJ})_{FE}$ is the area of cross section of the fully expanded microjet

$$(S_{MJ})_{FE} = \frac{\pi d_{MJ}^2}{4} (M_{MJ})_{FE}^{-1} \left[\frac{2}{\gamma + 1} \left(1 + \frac{\gamma - 1}{2} (M_{MJ})_{FE}^2 \right) \right]^{0.5(\gamma + 1)/(\gamma - 1)} \quad (\text{A.3})$$

In Eq. (A.3), γ is the specific heats ratio, d_{MJ} is the exit diameter of the supply pipe, and $(M_{MJ})_{FE}$ is the fully expanded Mach number

$$(M_{MJ})_{FE} = \left\{ \frac{2}{\gamma - 1} \left[\frac{\gamma + 1}{2} \left(\frac{p_{MJ}}{p_0} \right)^{(\gamma - 1)/\gamma} - 1 \right] \right\}^{1/2} \quad (\text{A.4})$$

Finally, the parameters at the exit of the microjet supply pipes needed to compute $(M_{MJ})_{FE}$ and the fully expanded parameters entering Eq. (A.2) are calculated based on a prescribed (e.g., known from experiment) value of the microjets mass flow rate, Q_{MJ} , and their stagnation temperature, $T_{MJ}^{(0)}$, assuming that the exit temperature of the microjets T_{MJ} is equal to the critical value, i.e., $T_{MJ} = 2T_{MJ}^{(0)}/(\gamma + 1)$.

As far as the source shape function $\Psi(\mathbf{r})$ is concerned, after a series of numerical experiments with different shapes and levels of smoothing at the boundaries, we arrived at the spherical shape of $\Psi(\mathbf{r})$ with the following distribution inside the sphere:

$$\Psi(\mathbf{r}) = \cos^3 \left[\frac{\pi}{2} \min \left(\frac{|\mathbf{r} - \mathbf{r}_0|}{\Delta r_0}, 1 \right) \right] \quad (\text{A.5})$$

where the vector \mathbf{r}_0 defines the position of the supply pipe exit and Δr_0 is the source “radius” which is set equal to one and a half times the radius of the fully expanded microjet, $(R_{MJ})_{FE} = [(S_{MJ})_{FE}/\pi]^{1/2}$. This results in “generation” of nearly uniform microjets with the “core” values close to the prescribed fully expanded parameters. Other source shapes we considered (cylinder, truncated cones) resulted in significant pressure gradients and high velocities in the radial direction, which, in turn, caused a pronounced widening of the generated microjet. Sharpening of the spatial distribution (A.5) leads to similar undesirable effects.

References

- [1] M.L. Shur, P.R. Spalart, M.Kh. Strelets, A.V. Garbaruk, Further steps in LES-based noise prediction for complex jets, AIAA Paper, AIAA-2006-485, 2006.
- [2] D. Eschricht, B. Greschner, F. Thiele, M.C. Jacob, Numerical simulation of jet mixing noise associated with engine exhausts, *Notes on Numerical Fluid Mechanics and Multidisciplinary Design* 104 (2009) 121–146. doi:10.1007/978-3-540-89956-3_6.
- [3] H. Xia, P.G. Tucker, S. Eastwood, Large-eddy simulations of chevron jet flows with noise predictions, *International Journal of Heat and Fluid Flow* 30 (2009) 1067–1079. doi:10.1016/j.ijheatfluidflow.2009.05.002.
- [4] S. Mendez, M. Shoeybi, A. Sharma, F.E. Ham, S.K. Lele, P. Moin, Large-eddy simulations of perfectly-expanded supersonic jets: quality assessment and validation. AIAA Paper, AIAA-2010-271, 2010.
- [5] M.L. Shur, P.R. Spalart, M.Kh. Strelets, Noise prediction for increasingly complex jets. Part I, Methods and tests; Part II, Applications, *International Journal of Aeroacoustics* 4 (2005) 213–266. doi:10.1260/1475472054771376 and 10.1260/1475472054771385.
- [6] M.L. Shur, P.R. Spalart, M.Kh. Strelets, A.V. Garbaruk, Analysis of jet-noise-reduction concepts by large-eddy simulation, *International Journal of Aeroacoustics* 6 (2007) 243–285. doi:10.1260/147547207782419561.
- [7] P.R. Spalart, M.L. Shur, Variants of the Ffowcs Williams-Hawkings equation and their coupling with simulations of hot jets, *International Journal of Aeroacoustics* 8 (2009) 477–492. doi:10.1260/147547209788549280.
- [8] A. Uzun, M.Y. Hussaini, High-fidelity numerical simulation of a chevron nozzle jet flow, AIAA Paper, AIAA-2009-3194, 2009.
- [9] P.R. Spalart, M.L. Shur, M.Kh. Strelets, Added sound sources in jets; theory and simulation, *International Journal of Aeroacoustics* 8 (2009) 511–534. doi:10.1260/147547209789141515.
- [10] K. Viswanathan, Aeroacoustics of hot jets, *Journal of Fluid Mechanics* 516 (2004) 39–82. doi:10.1017/S0022112004000151.
- [11] F.J. Harris, On the use of windows for harmonic analysis with the discrete Fourier transform, *Proceedings of the IEEE* 66 (1978) 51–83, doi: 10.1109/PROC.1978.10837.
- [12] J.C. Lau, Effects of exit Mach number and temperature on mean-flow and turbulence characteristics in round jets, *Journal of Fluid Mechanics* 105 (1981) 193–218. doi:10.1017/S0022112081003170.
- [13] J.C. Lau, P.J. Morris, M.J. Fisher, Measurements in subsonic and supersonic free jets using a laser velocimeter, *Journal of Fluid Mechanics* 93 (1979) 1–27. doi:10.1017/S0022112079001750.
- [14] V.H. Arakeri, A. Krothapalli, V. Siddavaram, M.B. Alkislal, L.M. Lourenco, On the use of microjets to suppress turbulence in a Mach 0.9 axisymmetric jet, *Journal of Fluid Mechanics* 490 (2003) 75–98. doi:10.1017/S0022112003005202.
- [15] J.C. Simonich, S. Narayanan, T.J. Barber, M. Nishimura, Aeroacoustic characterization, noise reduction and dimensional scaling effects of high subsonic jets, *AIAA Journal* 39 (2001) 2062–2069. doi:10.2514/2.1228.
- [16] A. Uzun, M.Y. Hussaini, Simulation of noise generation in near-nozzle region of a chevron nozzle jet, *AIAA Journal* 47 (2009) 1793–1810. doi:10.2514/1.36659.
- [17] K. Viswanathan, M.L. Shur, P.R. Spalart, M.Kh. Strelets, Flow and noise predictions for single and dual-stream beveled nozzles, *AIAA Journal* 46 (2008) 601–626. doi:10.2514/1.27299.
- [18] A. Krothapalli, B. Greska, V. Arakeri, High speed jet noise reduction using microjets, AIAA Paper, AIAA-2002-2450, 2002.
- [19] B. Greska, A. Krothapalli, N. Burnside, W. Horne, High-speed jet noise reduction using microjets on a jet engine, AIAA Paper, AIAA-2004-2969, 2004.
- [20] M.B. Alkislal, A. Krothapalli, G.W. Butler, The effect of streamwise vortices on the aeroacoustics of a Mach 0.9 jet, *Journal of Fluid Mechanics* 578 (2007) 139–169. doi:10.1017/S0022112007005022.
- [21] T. Castelain, M. Sunyach, D. Juve, J.-C. Bera, Jet-noise reduction by impinging microjets: an acoustic investigation testing microjet parameters, *AIAA Journal* 46 (2008) 1081–1087. doi:10.2514/1.29411.
- [22] E. Laurendeau, P. Jordan, J.P. Bonnet, J. Delville, P. Parnaudeau, E. Lamballais, Subsonic jet noise reduction by fluidic control: the interaction region and the global effect, *Physics of Fluids* 20 (2008) 101519. doi:10.1063/1.3006424.
- [23] M. Huet, F. Vuillot, G. Rahier, Numerical study of the influence of temperature and micro-jets on subsonic jet noise, AIAA Paper, AIAA-2008-3029, 2008.
- [24] M. Huet, D. Fayard, G. Rahier, F. Vuillot, Numerical investigation of the micro-jets efficiency for jet noise reduction, AIAA Paper, AIAA-2009-3127, 2009.
- [25] P.-T. Lew, A. Najafiyazdi, L. Mongeau, Unsteady numerical simulation of a round jet with impinging microjets for noise suppression, AIAA Paper, AIAA-2010-18, 2010.